Surface Activity of Early Transition Metal Oxycarbides: CO_2 Adsorption Case Study

Christian Kunkel,[†, ‡] Francesc Viñes,[†,*] and Francesc Illas[†]

[†] *Departament de Ciència de Materials i Química Fisica & Institut de Química Teòrica i Computacional (IQTCUB), Universitat de Barcelona, Martí i Franqués 1-11, 08028 Barcelona, Spain.*

[‡] *Chair for Theoretical Chemistry and Catalysis Research Center, Technische Universiät München, Lichtenbergstr. 4, D-85747 Garching, Germany.*

ABSTRACT

Theoretical studies and experiments have suggested that transition metal carbides (TMCs) can be useful materials for carbon capture and storage or use technologies from air sources. However, TMCs are known to become easily oxidized in the presence of molecular oxygen, and their properties jeopardized while being transformed into transition metal oxycarbides (TMOCs), which can affect the TMCs chemical activity, *e.g.* towards CO_2. Here, by means of density functional theory (DFT) based calculations including dispersion we address the possible effect of oxycarbide formation in the CO_2 capture course. A careful analysis of different models show that for group 4 TMCs (TM = Ti, Zr, Hf), their oxidation into TMOCs involves a negligible structural distortion of the outermost oxide surface layer, whereas severe rumplings are predicted for group 5 and 6 TMOCs (TM = V, Nb, Ta, Mo). The large surface distortion in the latter TMOCs results in a weak interaction with CO_2 with adsorption energies below -0.27 eV. On the contrary, on group 4 TMOCs surfaces CO_2 adsorption becomes stronger, with the adsorption values strengthening by 0.44-1.2 eV, a fact that, according to adsorption/desorption rates estimates, increments the air CO_2 capture temperature window by 175-400 K. The present DFT results point to group 4 TMCs, TiC in particular, as promising materials for air CO_2 capture and storage/conversion, even in the presence of oxygen and the possible formation of transition metal oxycarbides.

* Corresponding author: francesc.vines@ub.edu

1. INTRODUCTION

The chemistry of CO_2 when adsorbed on a materials surface is nowadays an active field of research,[1,2] highly spurred by the urgent necessity to find candidate materials able to efficiently capture CO_2, with the ultimate purpose of climate change mitigation.[3] Such materials must enable the implementation of CO_2 capture and storage (CSS) technologies,[4,5] and when possible, the CO_2 conversion into other greener added-value chemicals, through the so-called CO_2 capture and usage (CCU) processes. However, because of the high chemical stability of CO_2, only a few selected privileged materials are able to strongly enough adsorb CO_2 so that its capture is efficient under standard conditions of temperature and CO_2 partial pressure. Furthermore, CCU processes normally involve molecular activation, achievable *via* electron transfer from the substrate, leading to a bent CO_2 molecule with elongated, weakened C-O bonds,[1] which severely restricts the number of potential materials for this purpose.

Transition metal carbides (TMCs) have been recently adverted as potential materials for CCS and CCU technologies, with promising results based on density functional theory (DFT) simulations coupled to the transition state theory (TST) framework. These allowed gaining reasonable estimates of adsorption and desorption rates, and by so, of the practical CO_2 partial pressure and temperature windows.[6] Earlier DFT results pointed at CO_2 activation on molybdenum carbides on different stable surfaces,[7,8] where experimental results on different molybdenum carbide phases[8-10] revealed CO_2 dissociation at room temperature, together to a catalytic CO_2 hydrogenation conversion at elevated temperatures. This indirectly already evidenced the formation of surface activated CO_2 moieties. The prognosticated CO_2 adsorption and activation on TMCs most stable (001) surfaces[6] has been recently concept-proven by X-ray photoemission spectroscopies (XPS) based on the outcome of DFT simulated surface science techniques.[11] Note in passing by that two-dimensional early transition metal carbides, known as MXenes, have been likewise recently forecasted as appealing materials for CCS and CCU,[12] and the CO_2 selective capture in N_2/CO_2 mixtures recently experimentally confirmed.[13]

Despite the promising CCS/CCU features of most stable (001) surfaces of rocksalt crystal structure TiC, ZrC, HfC (group 4), NbC, TaC (group 5), and δ-MoC (group 6) TMCs,[6,11] one has to keep in mind that these materials are longstanding known to be easily oxidized, forming surface oxide structures known as oxycarbides. Thus, oxygen is regarded as a poison on TMCs,[14-16] *e.g.* oxycarbide is known to undermine the Mo_2C catalytic performance for the water gas shift (WGS) reaction, where O moieties are mostly created from the H_2O decomposition or hydroxyl recombination. In the course of the reverse WGS, either a direct hydrogenation of CO_2, or a rapid hydrogenation of as-created O adatoms may

prevent such oxycarbide formation, as observed on α-Mo_2C.[8] However, for the aforementioned series of TMCs, the interaction with O_2 often leads to dissociation with the potential formation of oxycarbides being greatly energetically and kinetically enhanced.[17-19] This is clearly exemplified in the WGS on TiC (001), where O adatoms are found to lead to a thermodynamic sink.[20]

The DFT calculated energy barriers, E_b, for O_2 dissociation go from very low on group 4 TMCs, ranging from 0.16 to 0.19 eV, to moderate on group 5 TMCs —0.47-0.82 eV—, being δ-MoC the most resilient, with an energy barrier of 1.15 eV.[17] Brønsted–Evans–Polanyi (BEP) relations predicted that TMCs would dissociate O_2 easier than extended and vicinal metal surfaces, and comparable to transition metal oxides.[21] Once O adatoms are present at the surface, DFT simulations combined with XPS data obtained for O on TiC and ZrC (001) surfaces showed that the C↔O exchange is an exothermic process, with calculated reaction energies of -1.1 and -0.68 eV for TiC and ZrC, at an O coverage (θ_O) of 0.25 monolayers (ML), respectively.[22,23] The C↔O exchange E_b was explicitly considered for the TiC (001) surface, showing that two O adatoms can act cooperatively to replace one surface C by an O atom, with a reduced energy barrier of 0.6 eV.[23] Therefore, it is reasonable to argue that such atomic exchange, with concomitant formation of an oxycarbide surface, is likely to occur under standard catalytic working conditions, unless is avoided, *e.g.* hydrogenating the as-generated the surface O. Aside, these previous studies support that surface generated O adatoms will eventually replace C in the carbide crystallographic network, rather than staying as an oxygen overlayer.

Clearly, a remaining open question concerns the impact of the formation of such oxycarbides in comparison to the chemistry of the pristine carbide surfaces. Along this discussion, the oxycarbide activity is often regarded as similar to the parent higher oxide situation, *e.g.*, the oxycarbide phase of TiC would chemically act similar to TiO_2,[8] although locally the oxycarbide geometric (and consequently electronic) structure can grossly differ from that of the parent bulk oxides. Furthermore, often the oxycarbide modeling is considered with fully O-covered TMC surfaces (θ_O = 1 monolayer)[16,24] with just rare exceptions where a fully oxidized TMC layer is duly described.[22,23] Hence, the surface chemistry of the oxycarbide phases resulting from exposing TMCs surfaces to oxygen remains essentially hitherto unknown.

In the present work, we contribute unraveling the impact of oxycarbide formation on the CCS activity of TMCs and, hence, to determine whether these materials would feature deactivation towards CO_2 in the presence of atmospheric O_2. To this end, we assume a limiting oxycarbide formation situation where the exposed TMC (001) surface has fully

exchanged its C atoms by O, *i.e.*, featuring a transition metal oxide layer but commensurate with atomic structure of the underlying TMC. Note, however, that such models suppose a layer-by-layer oxide growth from the parent carbide. However, one has to keep present that other mechanism may occur, such as pit growth, plus different domains with different oxide stoichiometries can coexist on a formed oxycarbide, here not tackled.

The here presented simulations, carried out by means of periodic DFT calculations on appropriate oxycarbide slab models of the (001) surface of these TMCs, show that group 4 transition metal oxycarbides (TMOCs) feature no significant surface relaxation, and by that they keep the CO_2 adsorptive and activation capabilities. The group 5 and 6 TMOCs either show no rumpling or partial/full oxygen rumpling, but in any case with very weak interaction with CO_2. Consequently, group 4 TMCs (TiC, ZrC, and HfC) are highlighted as materials for CO_2 CCS and CCU technologies even in the presence of O_2.

2. COMPUTATIONAL DETAILS

The studied TMOCs have been represented by periodic slab models The employed slabs are built from TMCs (001) surface models previously optimized with the same DFT based method,[6] but replacing the first layer C atoms by O atoms. These slab models contain four atomic layers with the two outermost fully relaxed and the two bottommost fixed as in the bulk optimized material, providing an appropriate environment to the surface region.[6] The structural optimizations are carried out within the same computational framework earlier described in the literature[6] using the Vienna *ab initio* simulation package (VASP),[25] and using the Perdew-Burke-Ernzerhof (PBE) exchange-correlation functional,[26] as it constitutes one of the most accurate choices in the description of TMCs.[27] Whenever necessary, the effect of dispersion related interaction terms, as in the estimate of CO_2 adsorption energies, have been included following the Grimme D3 (PBE-D3) correction.[28] The effect of the atomic core electrons on the valence electron density is taken into account through the projected augmented wave (PAW) method developed by Blöchl,[29] as implemented in VASP by Kresse and Joubert.[30] The valence electron density is expanded in a plane wave basis set, with a kinetic energy cutoff of 415 eV.

To speed-up the CO_2 adsorption calculations, an initial screening of all sites on the different surface models was carried out using a 5×5×1 Monkhorst-Pack **k**-points grid,[31] where most stable situations were refined reoptimized using a denser 9×9×1 grid. Convergence criteria for electronic and structural updates were 10^{-6} eV and 0.01 eV $Å^{-1}$ respectively. The adsorbed CO_2 optimized geometries were characterized as minima of the potential energy surface by frequency analysis through Hessian matrix construction and

diagonalization, with the elements of the adsorbate related Hessian matrix estimated from finite differences of analytical gradients with atomic displacements of 0.03 Å length. In some CO_2 physisorbed cases, one or two small spurious imaginary frequencies remain; always well below 50 cm^{-1}, and related to substrate non-fully frustrated translational or rotational modes. At the strict convergence criteria used, these geometries can be safely reported as minima of the potential energy surface.[32,33]

The interaction between CO_2 and the TMOC surfaces has been further studied by means of charge density difference (CDD) analysis, simulation of the associate infrared (IR) spectrum, and electron localization functions (ELF); computational details on these methods simulations can be found elsewhere.[11] Note that although the employed models describe oxycarbides with a full monolayer (ML) of oxygen coverage (θ_O = 1 ML), the CO_2 coverage considered is low enough (θ_{CO_2} = 0.125 ML) so as to disregard lateral interactions between periodically repeated CO_2 adsorbates. We should remind that for either O or CO_2, the coverage is defined as the number of entities with respect to the number of transition metal atoms exposed on the surface. The CO_2 adsorption energies, $E_{ads}^{CO_2}$, are estimated as

$$E_{ads}^{CO_2} = E_{CO_2/TMOC} - (E_{CO_2} + E_{TMOC}) \quad (1),$$

where $E_{CO_2/TMOC}$ is the energy of the TMOC (001) surface slab with the adsorbed CO_2, E_{TMOC} is the energy of the optimized yet pristine TMOC (001) surface slab, and E_{CO_2} the energy of the CO_2 molecule optimized in an asymmetric unit cell of 9×10×11 Å dimensions. Within this definition, the more negative the E_{ads}, the stronger the adsorption is. Unless stated otherwise, all reported E_{ads} values include the zero point energy (ZPE) correction. On the basis of the calculated harmonic vibrational frequencies, adsorption/desorption rates for CO_2 from the different surfaces have been obtained in the framework of TST as described in previous works.[6,32,33] For a fair comparison between TMC and TMOC surfaces —exhibiting different adsorption sites for CO_2—, a value of 0.139 nm^2 was used for an estimate of the adsorption site area on all surfaces. In addition, a conservative sticking factor of 0.2 was assumed for the CO_2 impingement on both TMC and TMOC surfaces.[32,33]

3. RESULTS AND DISCUSSION

3.1. Pristine TMOCs (001) surfaces

First, we consider the energetics and geometric structure of the TMOC (001) surfaces represented by the described slab models. Three different situations have been considered for each pristine TMOC surface, summarized in Figure 1. The first one corresponds to a structure with no (large) rumpling for the O atoms, the second one involves a structure where half of

the O atoms exhibit a rumpling in an alternating sequence along [011] surface planar directions, and the third one where the full O oxycarbide layer undergoes a severe rumpling. For each TMOC (001) surface Table 1 reports the surface energy difference between the optimized structure for each three models relative to the most stable one. Note that after relaxation some surface models evolved to different structures, *i.e.* the half rumpled situations for group IV TMOCs relaxed to the non-rumpled model. For all the other cases, the structures remained as such yet relaxed, being indeed minima of the potential energy landscape.

Analyzing the results, for group 4 TMOCs, the oxycarbide formation does not lead to any noticeable rumpling, as the full rumpling situations are higher in energy, with the sole exception of HfC oxycarbide, for which both surface structures are close in energy. The unrumpled, half-rumpled, and fully- rumpled situations are competitive in the (group 5) VC oxycarbide, whereas the fully rumpled situation appears to be the likely model for the rest of group 5 and 6 TMOCs. Note in passing by that even though unrumpled situations were explicitly optimized for group 5 and 6 TMOCs, these could spontaneously evolve to fully rumpled in the course of CO_2 adsorption.

The degree of rumpling can be quantified by measuring the O and TM heights of the TMOCs models compared to the parent TMC (001) surfaces.[6,34] The corresponding displacements, Δh, obtained from PBE geometry optimizations, are displayed in Table 2, and reveal how small these are for the the unrumpled situations, with displacements ranging from 0.04 to 0.07 Å for O atoms, -0.09 to -0.07 Å for TM atoms, whereas these displacements are much more acute on the fully rumpled situations, with O variations in the 0.84-1.06 Å range, although not so accentuated for TMs —0.04-0.14 Å—. Including dispersion in the geometry optimizations (PBE-D3) reveals very little variations in such rumplings, with variations inward by 0.02 Å in average, and are therefore no further discussed. In the half-rumpled situations two sets of TM and O rumplings are involved, each set pointing towards a different direction, *i.e.*, the unrumpled or the full-rumpled. According to the structural changes, it appears that group 5 and 6 TMOCs have more propensity towards a severe surface reconstruction. This behavior may be understood from the tendency to adopt the crystallographic environment of the corresponding bulk oxide, *e.g.* towards V_2O_5, Nb_2O5, Ta_2O_5, and MoO_3, which display orthorhombic crystal structures. Note, however, that this argument does not hold for group 4 TMOCs where, in spite of the tetragonal crystal structure of TiO_2, ZrO_2, and HfO_2, the rocksalt structure of TiC, ZrC, and HfC prevails with important consequences concerning CO_2 adsorption, as discussed below.

3.2. CO_2 adsorption

Following a previous procedure,[6] the CO_2 molecule has been adsorbed on the TMOCs slab models, by placing the molecule parallel to the surface, at a height of 1.6 to 2 Å, over different high-symmetry surface positions, contemplating top, bridge, and hollow positions, with two different CO_2 orientations along the surface planes on each site (see Figure 2). The geometry optimizations lead to two distinct situations depending on the TM group. On group 5 and 6 TMOCs, the geometry optimization of the adsorbed CO_2 on the fully rumpled models (NbC, TaC, and δ-MoC oxycarbides), and on the competitive unrumpled, half-rumpled and fully-rumpled models of the VC oxycarbide lead to physisorption situations with E_{ads} values smaller than -0.05 eV (PBE), which are slightly larger (below -0.27 eV) when including dispersions (PBE-D3); a summary of results is presented in Table 3. In these cases, the CO_2 molecule remains essentially straight and parallel to the surface, see Figure S3 in SI and structural data in Table 3, in line with the results for other surfaces where CO_2 interaction is weak. Hence, the above-commented rumpling, which brings the structure closer to the parental transition metal oxides, makes the positively charged metal centers less accessible to stabilize the negatively charged O atoms of an hypothetical $CO_2^{\delta-}$ entity, which seems to be key point in the predicted CO_2 *physisorption*.

However, the situation is markedly different for group 4 TMOCs, where a few competitive *chemisorption* situations are found. Figure 3 displays the most stable adsorption situation on TiOC, while the corresponding situations for HfOC and ZrOC are reported in the Figures S1 and S2 of the Supporting Information (SI), respectively. The molecular structure of the chemisorbed CO_2 on these TMOCs surfaces closely resembles those obtained on non-oxidized pristine TMC (001) surfaces.[6] However, here most cases involve a four-fold atom coordination, or indentation. In the case of TiOC, the most stable coordinations correspond to MOMO bidentate and tridentate sites, as shown in Figure 3. The most stable configuration for CO_2 on ZrOC displays the same MOMO tridentate as on TiOC but also another distinct tridentate MMMO situation (see Figure S1 in SI) is found. Notice also that CO_2 adsorbed on HfOC displays two types of MOMO tridentate configurations, hereafter referred to as symmetric and asymmetric, plus the MMMO tridentate situation. In all such chemisorbed states the CO_2 molecule gets activated with an OCO angle, α(OCO), in the 119.5-135.6º range, and with elongated C-O bond lengths, *d*(C-O), reaching 1.23-1.49 Å, remarkably larger than the isolated, gas phase, linear CO_2 molecule where *d*(C-O)= 1.18 Å (Table 3).

However, the most significant result is that the adsorption energy on group 4 TMOC (001) surface models is *larger* than the corresponding values for CO_2 adsorbed on the pristine TMC (001) ones. On the most stable configurations for CO_2 on the TiC, ZrC, and HfC

oxycarbides, already the PBE calculated $E_{ads}^{CO_2}$ values are -1.01, -2.03, and -2.66 eV, hence sensibly larger than for the most stable site TopC values on the parent carbides, computed to be -0.57, -1.39, and -1.42 eV, respectively.[6] This implies a noticeable enhancement of the interaction of -0.44, -0.64, and -1.38 eV for TiOC, ZrOC and HfOC, respectively. The larger $E_{ads}^{CO_2}$ values evidently comes from the coulombic part of the interaction since bonding in the oxycarbide layer is considerably more ionic than on the TMC parent material. Note also that the addition of van der Waals type of interactions through PBE-D3, simply implies an almost constant lowering of the bond strength by 0.22 to 0.28 eV, as previously seen on TMC (001) surfaces.[6]

The above interpretation is further supported by the Bader charge analysis, which reveals large TMOC→CO_2 charge transfers in the 1.0-1.9 *e* range, as gathered in Table 3. Note also that charge density difference (CDD) and electron localization function (ELF) profiles are similar to those corresponding to activated CO_2 on TMC (001) surfaces,[11] as shown in Figure 3. The present CDD pictures are fully consistent with surface metal and O centers favorably interacting with the Lewis acidic and basic carbon and oxygen atoms of CO_2.[35] Furthermore, charge depletion at the TMOC surface and charge accumulation regions on the CO_2 molecule support the charge transfer mechanism above discussed. Finally, the ELF plots highlight an important electron pair density between the oxycarbide surface O atom directly involved in the CO_2 adsorption and the CO_2 carbon atom, evidencing a newly formed covalent bond, and therefore suggesting the emergence of a carbonate (CO_3^{2-}) type of entity. Such carbonate-type of interaction is classically observed for CO_2 when chemisorbed on highly ionic rocksalt alkaline earth oxides, such as MgO or CaO, where previous studies showed that the CO_2 adsorbs in a monodentate and tridentate fashion as the here exposed TopO and MMO sites on TiOC.[36,37] This goes along with the observed interaction of CO_2 on the rocksalt type of titanium dioxide, as TiO is known to be more ionic than titanium dioxide TiO_2,[38] and hence, behaving quite as an alkaline earth oxide such as MgO or CaO.

3.3. Consequences on CCS and CCU

According to the calculated CO_2 adsorption energies on the oxycarbide models described in the previous, the oxidation of TMC (001) surfaces would unchain dramatic consequences for most of the systems. While group 5 and 6 NbC, TaC, and δ-MoC will chemisorb and activate CO_2 at normal conditions of temperature and CO_2 partial pressure[6] — even VC if exposed to sufficiently high partial pressure[11]—, a point experimentally observable by infrared (IR) spectroscopies with signals in the 1100-1600 cm^{-1} range,[11] the

corresponding oxidized (VOC, NbOC, TaOC and MoOC oxycarbide) surfaces would lead to physisorbed CO_2, and, therefore, to no IR active signals. On the contrary, the formation of the TiOC, ZrOC, and HfOC oxycarbides would just imply a shift of the IR active bands as shown in Figure 4. Given the distorted nature of the CO_2 bonding in these oxycarbide surface models, the shift appears to be especially significant in the asymmetric stretching, ν_{as}, of the C-O bonds. As an example, the TopC CO_2 adsorption IR feature on TiC (001) surface, predicted to be centered at 1514 cm^{-1}, which would significantly blueshift by 128 cm^{-1} on TopO situation to a value of 1642 cm^{-1}, see Figure 4. On the contrary, the symmetric stretching, ν_s, would barely redshift by 18 cm^{-1}. In this sense vibrational spectroscopies would constitute a straightforward way of detecting and distinguishing activated CO_2 on carbide and oxycarbide surfaces, or, alternatively, to detect the presence of surface oxidation of a TMC using CO_2 as a probe molecule.

Last, the noticeable strengthening of the CO_2 adsorption on group 4 TMOC (001) surfaces has consequences on the transition temperature ranges for switching from CO_2 capture to release, which would move to values higher than for the corresponding TMC. This is shown on Figure 5 for most stable CO_2 adsorption on group 4 TMOCs, with adsorption/desorption rates estimated from transition state theory[6] and considering the ZPE-corrected PBE and PBE-D3 adsorption energies as fringe situations. Within this procedure we evaluated the turning temperatures for three CO_2 partial pressures (P_{CO_2}); *i)* the nowadays atmospheric CO_2 partial pressure of 40 Pa,[39] *ii)* a $P_{CO_2} = 15 \cdot 10^3$ Pa pressure benchmark used in exhaust gases,[40] and *iii)* a standard pressure of 1 bar (10^5 Pa), relevant in the pure CO_2 stream generation after CCS.[41] The results reveal that, under O_2 atmospheric conditions, CO_2 would be stronger adsorbed on the TMOCs than on the TMCs and, hence, it will be more difficult to be released. Note that going from TMC to TMOC shifts, the turning ranges increase by 150-190 K, and stretch over a wider range, even more acute in the HfC based case. Nevertheless, the higher surface activity of group 4 oxycarbides, their carbide passivating nature, and their enhanced CO_2 activation capabilities would make them excellent, realistic choices for the CO_2 posterior conversion, *e.g.*, for CO_2 hydrogenation towards methanol, although further research has to be devoted on this matter.

4. SUMMARY AND CONCLUSIONS

In this work TMOCs surface models have been built, analyzed, and used to study oxycarbide formation implications in the CO_2 adsorption and activation on the stable (001) surfaces of different transition metal carbides (TMCs). The structural optimizations on the TMOC (001) surface models carried out by means of appropriate DFT based methods reveal

that group 4 TMOCs (TM = Ti, Zr, Hf) show no significant rumpling of the surface atoms upon relaxation. However, a completely different result is found for group 5 (TM = V, Nb, Ta) and group 5 δ-MoOC where significant rumpling emerges, with either large displacements of surface O atoms towards the vacuum, or a line displacement of every second surface O atom along the [011] surface planar directions.

The large surface rumpling of group 5 and 6 TMOCs seems to point towards a transition metal, non-reducible, oxide surface-like chemical activity, which would explain the CO_2 physisorption situations with E_{ads} of at most -0.27 eV as obtained at PBE-D3 level. However, on group 4 TMOCs the parent carbide rocksalt crystallographic structure is almost preserved, which seems to maintain and even foster the CO_2 chemisorption with E_{ads} strengthened by 0.44-1.2 eV with respect to parent group 4 TMCs. Moreover, the appearance of the TMOC surface leads to a richer diversity of adsorption conformations, including MMMO and MOMO bidentate, tridentate, and tridentate asymmetric conformations.

The analysis of atomic and electronic structure of CO_2 adsorbed on group 4 TMOCs shows an activated bent molecular geometry, with elongated C-O bond lengths, and a charge transfer from the substrate to the molecule, in accordance with the results on TMCs. Estimates of TST adsorption/desorption rates reveal that the enhanced CO_2 adsorption would imply significant increases of 175-400 K in the lower limit transition temperature range in between CO_2 storage and release. The present calculations also show that CO_2 attachment on TMOCs, or even oxycarbide formation with CO_2 as a probe, can be monitored by IR spectroscopies, since simulated shifts of CO_2 on TMOC related features compared to TMCs can imply blue shifts ranging 106-188 cm^{-1} for the asymmetric CO_2 stretching.

All in all, the present DFT PBE-D3 simulations on transition metal oxycarbide surface models, implying a layer-by-layer oxycarbide formation, reveal that on group 5 and 6 TMCs oxycarbide formation would prevent the possible CO_2 capture and activation, and therefore, ultimately its conversion. On the contrary, on group 4 TMCs the CO_2 capture and activation can be enhanced by the oxycarbide formation, especially on going from TiC to TiOC. Given the proposed oxycarbide formation mechanism, the above results, together to the estimation of temperature ranges for CO_2 capture/release on group 4 TMOCs for different CO_2 partial pressures strongly suggest that these materials constitute good candidates for carbon capture and storage even in presence of oxygen, and the concomitant formation of an oxycarbide surface. Moreover, calculated vibrational frequencies of adsorbed CO_2 on TMC and TMOC suggest that IR can be used monitor both CO_2 adsorption on these two surfaces or the oxycarbide formation.

ASSOCIATED CONTENT

Supporting Information: Most stable CO_2 adsorbed geometries on the ZrOC and HfOC (001) surface slab models and the corresponding CDD plots (Figures S1 and S2, respectively) and most stable CO_2 physisorbed situations on the TMOC surface models (Figure S3). The Supporting Information is available free of charge on the ACS Publications website at DOI: XXXXXXXXXXX

ACKNOWLEDGEMENTS

This work was supported by Spanish *Ministerio de Economía y Competitividad* (MEC) CTQ2015-64618-R grant, *Generalitat de Catalunya* grants 2017SGR13 and XRQTC, and EU H2020 NOMAD project No 676580. F.V. thanks Spanish MEC for a *Ramón y Cajal* research contract (RYC-2012-10129). F.I. acknowledges additional support from the 2015 ICREA Academia Award for Excellence in Research. Financial support from Spanish MICIUN through the Excellence *María de Maeztu* program (grant MDM-2017-0767) is also fully acknowledged.

Table 1. Excess surface energy, γ, as obtained at PBE (-D3) level, relative to the most stable TMOC (001) surface model. Values are given in $J \cdot m^{-2}$.

γ	No rumpling	Half rumpling	Full rumpling
TiOC	**0.00**	←relaxation	1.19
ZrOC	**0.00**	←relaxation	0.61
HfOC	**0.03**	←relaxation	**0.00**
VOC	0.20	**0.00**	0.14
NbOC	0.65	0.34	**0.00**
TaOC	1.66	0.94[a]	**0.00**
δ-MoOC	1.48	0.54[a]	**0.00**

[a] The optimization leads to distortion of the surface.

Table 2. Rumpling change, Δ*h*, in Å, of TMOC surface atoms with respect to the parent TMC (001) surface models, as obtained at the PBE level. The Δ*h* values are given for each most stable TMOC surface (see Table 1) as the maximum height difference in the surface layer between (1) TMOC oxygen and TMC and carbon, Δ*h(O-C)*, and (2) TMOC and TMC transition metal atoms, Δ*h(TM-TM)*,. In the case of type *ii)* surface half rumpling, two sets of O and TM values are given.

Δ*h*	Surface type	Δ*h(O-C)*	Δ*h(TM-TM)*
TiOC	*i)*	0.07	-0.07
ZrOC	*i)*	0.06	-0.09
HfOC	*i)*	0.04	-0.07
HfOC	*iii)*	1.06	0.12
VOC	*ii)*	0.66/-0.03	-0.03
NbOC	*iii)*	1.06	0.14
TaOC	*iii)*	1.04	0.13
δ-MoOC	*iii)*	0.84	0.04

Table 3. Calculated properties for CO_2 adsorption on the oxycarbide surface models: Adsorption energies E_{ads} (in eV), net charge transfer ΔQ to CO_2 (in *e*), C-O bond lengths *d*(C-O) (in Å) and OCO angles α (in °). Adsorption energies at the PBE (-D3) level of theory include zero point energy (ZPE) contributions. *d* and α were obtained from the PBE optimized geometry, while the PBE-D3 deviated by at maximum 0.01 Å or 0.6°. The most stable adsorption on each oxycarbide —MOMO, MMMO, or 4-Hollow TM site, here 4-H TM) is marked in bold. The coordination (Coord.) is marked as bid (bidentated), trid (tridentated), sym (symmetric), and asym (asymmetric), and phys (physisorption).

	Site	Coord.	E_{ads} PBE (-D3)	ΔQ	*d*(C-O)	α
TiOC	MOMO	bid	-0.87 (-1.14)	-1.0	1.23/1.35	124.4
	MOMO	**trid-sym**	**-1.01 (-1.29)**	**-1.1**	**1.26**	**135.6**
ZrOC	MMMO	trid-sym	-1.72 (-1.94)	-1.4	1.31	120.4
	MOMO	**trid-sym**	**-2.01 (-2.25)**	**-1.2**	**1.28**	**129.3**
HfOC	MOMO	trid-asym	-2.56 (-2.79)	-1.9	1.31/1.49	119.5
type i)	MMMO	trid-sym	-2.35 (-2.57)	-1.4	1.32	119.5
	MOMO	**trid-sym**	**-2.66 (-2.92)**	**-1.3**	**1.28**	**128.5**
type iii)	**4-H TM**	**phys**	**-0.05 (-0.26)**	**0.0**	**1.18**	**178.7**
VOC	**TopO**	**phys**	**-0.03 (-0.27)**	**0.0**	**1.18**	**179.8**
NbOC	**4-H TM**	**phys**	**-0.04 (-0.25)**	**0.0**	**1.18**	**178.7**
TaOC	**4-H TM**	**phys**	**-0.04 (-0.26)**	**0.0**	**1.18**	**178.8**
δ-MoOC	**4-H TM**	**phys**	**-0.03 (-0.24)**	**0.0**	**1.18**	**179.1**

Figure 1. Exemplary views of *i)* a unrumpled —TiOC, left—, *ii)* half-rumpled —VOC, middle—, and *iii)* fully-rumpled —TaOC, right—, TMOC (001) surfaces. Grey and red spheres denote C and O atoms, whereas other colors represent the TM atoms. Lighter color layers were fixed at their bulk positions during surface relaxation and adsorption studies.

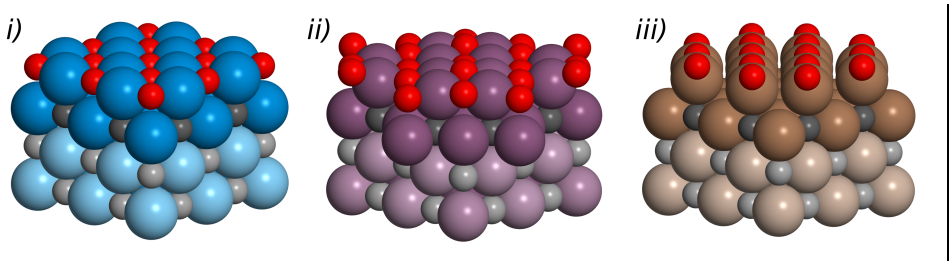

Figure 2. Sampled sites for CO_2 adsorption on (a) type *i)* or *ii)* surfaces and (b) on type *iii)* surface slab models. Color scheme as in Figure 1.

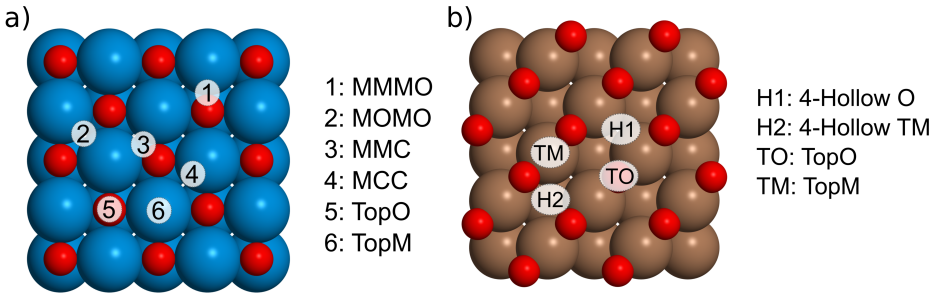

Figure 3. Most stable CO_2 adsorption geometries on the TiOC (001) surface models. Upper top left and right: CDD and ELF of these stable CO_2 adsorption geometries. The CDD show yellow (grey) isosurfaces denoting areas of charge accumulation (depletion), at an isovalue of 0.05 e/Å^3, for the bidentate and tridentate symmetric cases.

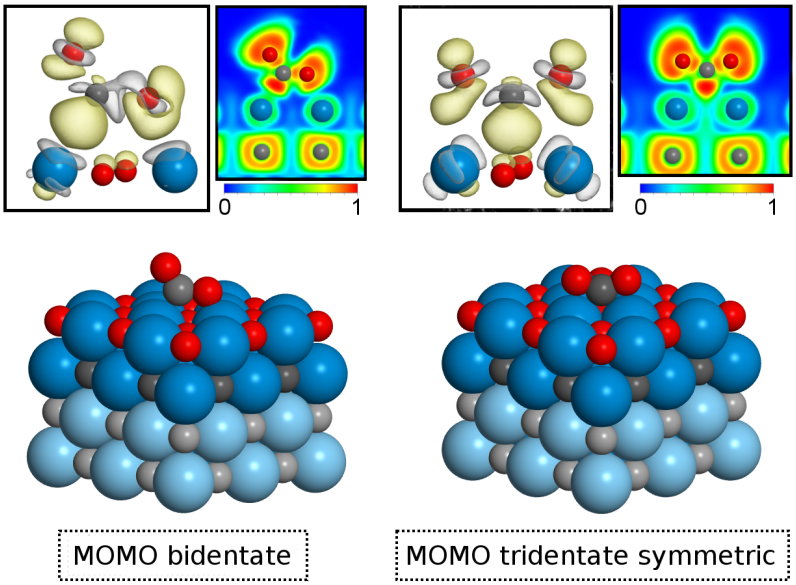

Figure 4. Simulated IR spectra of CO_2 adsorbed on the TiOC, ZrOC, and HfOC (001) surfaces. Peaks are marked with their vibrational frequency (in cm^{-1}). Relative intensities (Rel. int.) of the asymmetric stretch, ν_{as}, were overall low and have been slightly increased for better visibility.

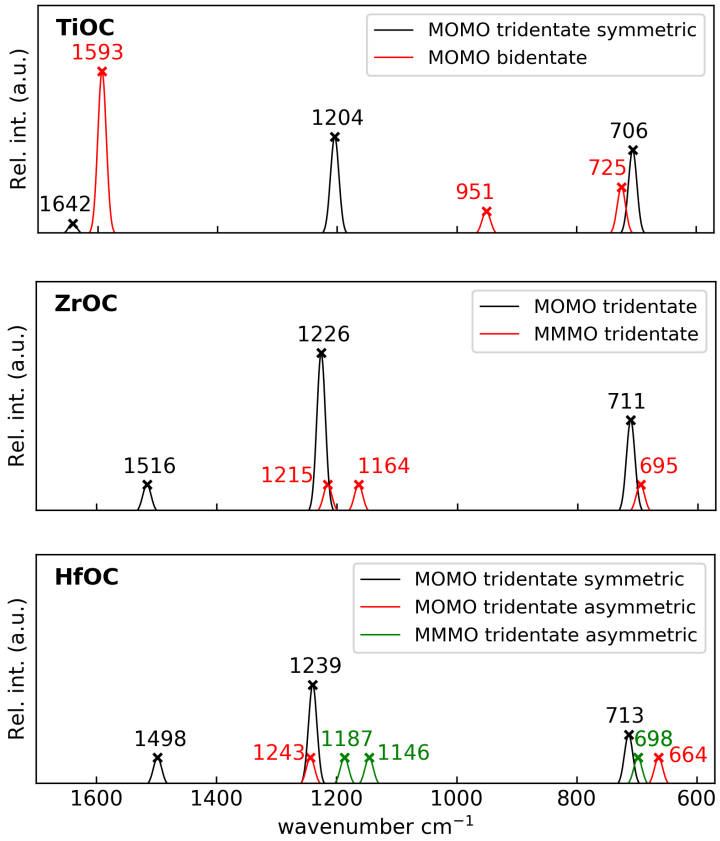

Figure 5. Calculated rates of adsorption, r_{ads}, and desorption, r_{des}, for CO_2 on TiOC, ZrOC, and HfOC (001) surface models as a function of the temperature, and at three partial pressures of CO2: 40, $15 \cdot 10^3$, and 10^5 Pa. For each adsorption situation, limiting values for strongest PBE-D3 (dotted lines) and weakest PBE chemisorption cases (solid lines) are considered. The marked points T_1-T_6 show how adsorption/desorption turning temperature ranges have been acquired (depicted below). For convenience, similar ranges are also shown for TiC, ZrC, HfC.

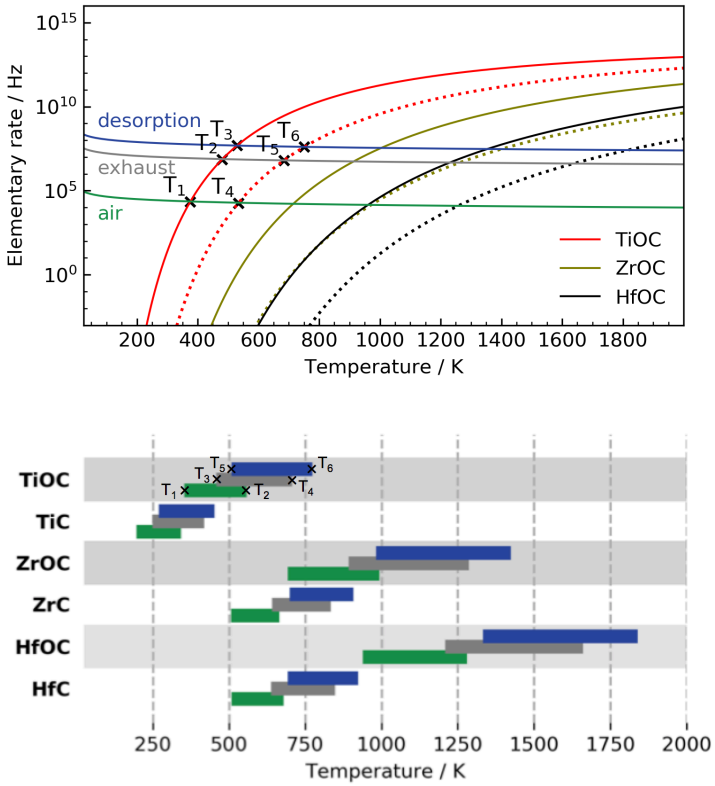

References

(1) Freund, H.; Roberts, M. W. Surface Chemistry of Carbon Dioxide. *Surf. Sci. Rep.* **1996**, *25*, 225–273.

(2) Taifan, W.; Boily, J.-F.; Baltrusaitis, J. Surface Chemistry of Carbon Dioxide Revisited. *Surf. Sci. Rep.* **2016**, *71*, 595–671.

(3) Edenhofer, O.; Pichs-Madruga, R.; Sokona, Y.; Minx, J. C.; Farahani, E.; Susanne, K.; Seyboth, K.; Adler, A.; Baum, I.; Brunner, S.; et al. *Climate Change 2014: Mitigation of Climate Change*; 2014.

(4) Espinal, L.; Poster, D. L.; Wong-Ng, W.; Allen, A. J.; Green, M. L. Measurement, Standards, and Data Needs for CO_2 Capture Materials: A Critical Review. *Environ. Sci. Technol.* **2013**, *47*, 11960–11975.

(5) D'Alessandro, D. M.; Smit, B.; Long, J. R. Carbon Dioxide Capture: Prospects for New Materials. *Angew. Chemie - Int. Ed.* **2010**, *49*, 6058–6082.

(6) Kunkel, C.; Viñes, F.; Illas, F. Transition Metal Carbides as Novel Materials for CO_2 Capture, Storage, and Activation. *Energy Environ. Sci.* **2016**, *9*, 141–144.

(7) Shi, Y.; Yang, Y.; Li, Y. W.; Jiao, H. Activation Mechanisms of H_2, O_2, H_2O, CO_2, CO, CH_4 and C_2H_x on Metallic $Mo_2C(001)$ as Well as Mo/C Terminated $Mo_2C(101)$ from Density Functional Theory Computations. *Appl. Catal. A Gen.* **2016**, *524*, 223–236.

(8) Liu, X.; Kunkel, C. R.; Ramirez De La Piscina, P.; Homs, N.; Viñes, F.; Illas, F. Effective and Highly Selective CO Generation from CO_2 Using a Polycrystalline α-Mo_2C Catalyst. *ACS Catal.* **2017**, *7*, 4323–4335.

(9) Porosoff, M. D.; Yang, X.; Boscoboinik, J. A.; Chen, J. G. Molybdenum Carbide as Alternative Catalysts to Precious Metals for Highly Selective Reduction of CO_2 to CO. *Angew. Chemie - Int. Ed.* **2014**, *53*, 6705–6709.

(10) Porosoff, M. D.; Kattel, S.; Li, W.; Liu, P.; Chen, J. G. Identifying Trends and Descriptors for Selective CO_2 Conversion to CO over Transition Metal Carbides. *Chem. Commun.* **2015**, *51*, 6988–6991.

(11) Kunkel, C.; Viñes, F.; Ramírez, P. J.; Rodriguez, J. A.; Illas, F. Combining Theory and Experiment for Multitechnique Characterization of Activated CO_2 on Transition Metal Carbide (001) Surfaces. *J. Phys. Chem. C* **2018**, 10.1021/acs.jpcc.7b12227.

(12) Morales-García, A.; Fernández-Fernández, A.; Viñes, F.; Illas, F. CO_2 abatement using two-dimensional MXene carbides. *J. Mater. Chem. A* **2018**, *6*, 3381-3385.

(13) Persson, I.; Halim, J.; Lind, H.; Hansen, T. W.; Wagner, J. B.; Näslund L.-Å.; Darakchieva, V.; Palisaitis, J.; Rosen, J.; Persson, P. O. Å. 2D Transition Metal Carbides (MXenes) for Carbon Capture. *Adv. Mater.* **2018**, 1805472.

(14) Hwu, H. H.; Chen, J. G. Surface Chemistry of Transition Metal Carbides. *Chem. Rev.* **2005**, *105*, 185–212.

(15) Moon, D. J.; Ryu, J. W. Molybdenum Carbide Water–Gas Shift Catalyst for Fuel Cell-Powered Vehicles Applications. *Catal. Lett.* **2004**, *92*, 17-24.

(16) Liu, P.; Rodriguez, J. A. Water-Gas-Shift Reaction on Molybdenum Carbide Surfaces: Essential Role of the Oxycarbide. *J. Phys. Chem. B* **2006**, *110*, 19418-19425.

(17) Viñes, F.; Sousa, C.; Illas, F.; Liu, P.; Rodriguez, J. A. A Systematic Density Functional Study of Molecular Oxygen Adsorption and Dissociation on the (001) Surface of Group IV−VI Transition Metal Carbides. *J. Phys. Chem. C* **2007**, *111*, 16982–16989.

(18) Viñes, F.; Sousa, C.; Illas, F.; Liu, P.; Rodriguez, J. A. Density Functional Study of the Adsorption of Atomic Oxygen on the (001) Surface of Early Transition-Metal Carbides. *J. Phys. Chem. C* **2007**, *111*, 1307–1314.

(19) Zhang, Y. F.; Viñes, F.; Xu, Y. J.; Li, Y.; Li, J. Q.; Illas, F. Role of Kinetics in the Selective Surface Oxidations of Transition Metal Carbides. *J. Phys. Chem. B* **2006**, *110*, 15454-15458.

(20) Viñes, F.; Rodriguez, J. A.; Liu, P.; Illas, F. Catalyst Size Matters: Tuning the Molecular Mechanism of the Water–Gas Shift Reaction on Titanium Carbide Based Compounds. *J. Catal.* **2008**, *260*, 103–112.

(21) Viñes, F.; Vojvodic, A.; Abild-Pedersen, F.; Illas, F. Brønsted–Evans–Polanyi Relationship for Transition Metal Carbide and Transition Metal Oxide Surfaces. *J. Phys. Chem. C* **2013**, *117*, 4168–4171.

(22) Rodriguez, J. A.; Liu, P.; Gomes, J.; Nakamura, K.; Viñes, F.; Sousa, C.; Illas, F. Interaction of Oxygen with ZrC(001) and VC(001): Photoemission and First-Principles Studies. *Phys. Rev. B* **2005**, *72*, 075427.

(23) Rodriguez, J. A.; Liu, P.; Dvorak, J.; Jirsak, T.; Gomes, J.; Takahashi Y.; Nakamura, K. The Interaction of Oxygen with TiC(001): Photoemission and First-Principles Studies. *J. Chem. Phys.* **2004**, *121*, 465.

(24) Cheng, L.; Li, W.; Chen, Z.; Ai, J.; Zhou, Z.; Liu, J. DFT Study of Oxygen Adsorption on Mo_2C(001) and (201) Surfaces at Different Conditions. *Appl. Surf. Sci.* **2017**, *411*, 394-399.

(25) Kresse, G.; Furthmüller, J. Efficient Iterative Schemes for Ab Initio Total-Energy Calculations Using a Plane-Wave Basis Set. *Phys. Rev. B* **1996**, *54*, 11169–11186.

(26) Perdew, J. P.; Burke, K.; Ernzerhof, M. Generalized Gradient Approximation Made Simple. *Phys. Rev. Lett.* **1996**, *77*, 3865–3868.

(27) Politi, J. R. D. S.; Viñes, F.; Rodriguez, J. A.; Illas, F. Atomic and Electronic Structure of Molybdenum Carbide Phases: Bulk and Low Miller-Index Surfaces. *Phys. Chem. Chem. Phys.* **2013**, *15*, 12617-12625

(28) Grimme, S.; Antony, J.; Ehrlich, S.; Krieg, H. A Consistent and Accurate Ab Initio Parametrization of Density Functional Dispersion Correction (DFT-D) for the 94 Elements H-Pu. *J. Chem. Phys.* **2010**, *132*, 154104.

(29) Blöchl, P. E. Projector Augmented-Wave Method. *Phys. Rev. B* **1994**, *50*, 17953–17979.

(30) Kresse, G.; Joubert, D. From Ultrasoft Pseudopotentials to the Projector Augmented-Wave Method. *Phys. Rev. B* **1999**, *59*, 1758–1775.

(31) Monkhorst, H. J.; Pack, J. D. Special Points for Brillouin-Zone Integrations. *Phys. Rev. B* **1976**, *13*, 5188–5192.

(32) Kunkel, C.; Viñes, F.; Lourenço, M. A. O.; Ferreira, P.; Gomes, J. R. B.; Illas, F. Selectivity for CO_2 over CH_4 on a Functionalized Periodic Mesoporous Phenylene-Silica Explained by Transition State Theory. *Chem. Phys. Lett.* **2017**, *671*, 161-164.

(33) Kunkel, C.; Viñes, F.; Illas, F. Biogas Upgrading by Transition Metal Carbides. *ACS Appl. Energy Mater.* **1**, *1*, 43-47.

(34) Viñes, F.; Sousa, C.; Liu, P.; Rodriguez, J. A.; Illas, F. A Systematic Density Functional Theory Study of the Electronic Structure of Bulk and (001) Surface of Transition-Metals Carbides. *J. Chem. Phys.* **2005**, *122*, 174709.

(35) Burghaus, U. Progress in Surface Science Surface Chemistry of CO_2 − Adsorption of Carbon Dioxide on Clean Surfaces at Ultrahigh Vacuum. *Prog. Surf. Sci.* **2014**, *89*, 161−217.

(36) Downing, C. A.; Sokol, A. A.; Catlow, C. R. A. The Reactivity of CO_2 on the MgO(100) Surface. *Phys. Chem. Chem. Phys.* **2014**, *16*, 184-195.

(37) Pacchioni, G.; Ricart, J. M.; Illas, F. Ab Initio Cluster Model Calculations on the Chemisorption of CO_2 and SO_2 Probe Molecules on MgO and CaO(100) Surfaces. A Theoretical Measure of Oxide Basicity. *J. Am. Chem. Soc.* **1994**, *116*, 10152-10158.

(38) Sousa, C.; Illas, F. Ionic-Covalent Transition in Titanium Oxides. *Phys. Rev. B* **1994**, *50*, 13974-13980.

(39) Takahashi, T.; Sutherland, S.; Kozyr, A. *Global Ocean Surface Water Partial Pressure of CO_2 Database: Measurements Performed During 1957-2014 (Version 2014)*, Environmental Sciences Division, Oak Ridge National Laboratory, **2015**.

(40) D'Alessandro, D. M.; Smit, B.; Long, J. R. Carbon Dioxide Capture: Prospects for New Materials. *Angew. Chem. Int. Ed.* **2010**, *49*, 6058-6082.

(41) Boot-Handford, M. E.; Abanades, J. C.; Anthony, E. J.; Blunt, M. J.; Brandani, S.; Mac Dowell, N.; Fernández, J. R.; Ferrari, M.-C.; Gross, R.; Hallett, J. P.; Haszeldine, R. S.; Heptonstall, P.; Lyngfelt, A.; Makuch, Z.; Mangano, E.; porter, R. T. J.; Pourkashanian, M.; Rochelle, G. T.; Shah, N.; Yao, J. G.; Fennell, P. S. Carbon Capture and Storage Uptake. *Energy Environ. Sci.* **2014**, *7*, 130-189.

TOC Graphic

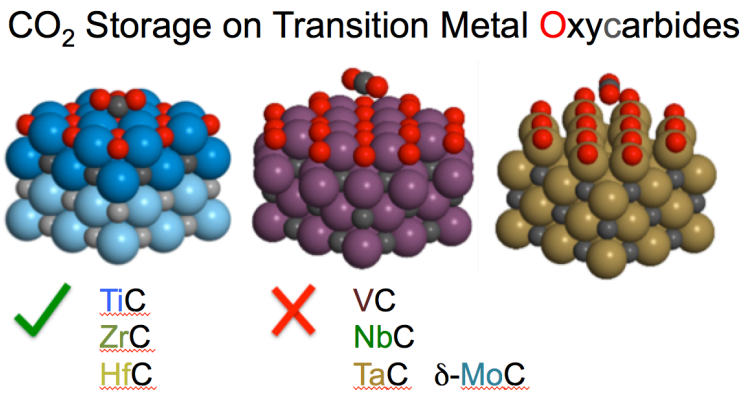
CO2 Storage on Transition Metal Oxycarbides
TiC
ZrC
HfC
VC
NbC
TaC
δ-MoC